High-temperature ferromagnetic $LaCoO_3$ triggered by interfacial electron transfer and exchange coupling

Yaoyao Ji,[1,*] Shilin Hu,[1,*] Junhua Liu,[1] Long Wei,[1] Chen Luo,[2] Victor Ukleev,[2] Florin Radu,[2] Wensheng Yan,[1] Dachuan Chen,[1] Zhicheng Zhong,[3] Yulin Gan,[1,†] Kai Chen,[1,‡] and Zhaoliang Liao[1,§]

[1]*National Synchrotron Radiation Laboratory, University of Science and Technology of China, Hefei 230026, Anhui, China*

[2]*Helmholtz-Zentrum-Berlin für Materialien und Energie, Hahn-Meitner Platz 1, D-14109 Berlin, Germany*

[3]*Suzhou Institute for Advanced Research of USTC, Suzhou 215123, China*

(Received 10 December 2023; accepted 26 April 2024; published 10 May 2024)

The perovskite oxide heterointerface is a complex and fascinating region where charge transfer dramatically alters the coupling between charge, spin, orbital, and lattice order, resulting in novel phenomena absent in bulk materials. Understanding and controlling these interfacial effects is crucial for designing and optimizing oxide heterostructures for potential applications. Specifically, charge transfer can stabilize and enhance the ferromagnetic order at the interface, effectively improving the properties of magnetic materials. In this work, a detailed investigation of the $LaCoO_3/La_{2/3}Sr_{1/3}MnO_3$ heterostructures revealed Mn-Co ferromagnetic coupling induced by charge transfer at the interface. Remarkably, this interfacial ferromagnetic coupling dramatically increased the Curie temperature of the $LaCoO_3$ film up to 190 K, which is significantly higher than the single $LaCoO_3$ film. Using surface-sensitive x-ray absorption spectra and x-ray magnetic circular dichroism, we find sizable Co^{2+} forms from the charge transfer between Mn-Co sites at the interface. Combined with density functional theory calculations, it is clear that the e_g^0-O-e_g^2 type Mn^{4+}-O-Co^{2+} superexchange interaction is at the root of the strong ferromagnetic coupling behavior. This work demonstrates that interface modulation in perovskite heterostructures can be a powerful tool for manipulating overall magnetism. It also underscores that perovskite oxide interfaces provide an ideal platform for exploring intricate interactions between different order parameters and inducing novel interfacial effects.

DOI: 10.1103/PhysRevB.109.174423

I. INTRODUCTION

Perovskite oxide heterojunctions attract extensive interest due to their diverse and intriguing physical phenomena, such as high mobility electron gas [1,2], metal-insulator transition [3], topological Hall effect [4], and superconductivity [5]. These phenomena are strongly sensitive to the interfacial effects, so the artificial heterointerface provides a new degree of freedom to modulate such remarkable properties effectively. Interfacial charge transfer is widely observed and causes charge redistribution among different perovskite compounds, leading to unique interfacial phenomena. Specifically, the interfacial effects in magnetic heterojunctions induced many emergent properties such as the exchange bias at the magnetic superlattices [6,7], the emergence of ferromagnetism in $SrMnO_3/SrIrO_3$ superlattices [8], and enhanced ferromagnetism at the $CaRuO_3/La_{0.67}Ca_{0.33}MnO_3$ interface [9].

Ferromagnetic insulators are vital for the advancement of novel magnetic devices, such as microwave devices [10], permanent magnets [11], magnetic tunneling junctions [12], and spintronic devices [13]. The $LaCoO_3$ (LCO) thin film is one type of ferromagnetic insulator with great potential, but its Curie temperature (T_C) is still too low for practical applications [14]. Compared to bulk LCO with a nonmagnetic ground state of Co^{3+} low spin (LS; $t_{2g}^6e_g^0$, $S=0$), the LCO film exhibits a T_C of approximately 90 K under tensile strain [15], with mixed spin states of Co^{3+} LS and Co^{3+} high spin (HS; $t_{2g}^4e_g^2$, $S=2$) [16]. Although the magnetic origin of the LCO films is still under debate, it is generally accepted that the $Co^{3+}-$HS state facilitates ferromagnetic ordering [17]. Leveraging the synergistic modulation of interfacial charge transfer as well as magnetic exchange coupling was considered a sufficient way to improve the ferromagnetic ordering temperature T_C of ultrathin LCO film.

Given the additional interfacial magnetic exchange coupling, it is reasonable to hypothesize that the ferromagnetism of ultrathin LCO film will be enhanced at the interface with ferromagnetic $La_{2/3}Sr_{1/3}MnO_3$ (LSMO), accompanied by the anticipated charge-transfer behavior. In this work, a high-quality LCO/LSMO heterostructure interface was created to enhance the T_C of the LCO layer. Investigations of the element-specific x-ray magnetic circular dichroism (XMCD) spectra at the Co and Mn L edges and temperature-dependent magnetization have revealed a ferromagnetic state of LCO with a T_C of 190 K. The reduction of Co^{3+} to Co^{2+} characterized by the x-ray absorption spectroscopy (XAS) suggests charge transfer from Mn to Co near the LCO/LSMO interface. Here, the enhanced T_C of LCO is caused by the Mn^{4+}-O-Co^{2+}

*These authors contributed equally to this work.
†Corresponding author: ylgan@ustc.edu.cn
‡Correpsonding author: kaichen2021@ustc.edu.cn
§Corresponding author: zliao@ustc.edu.cn

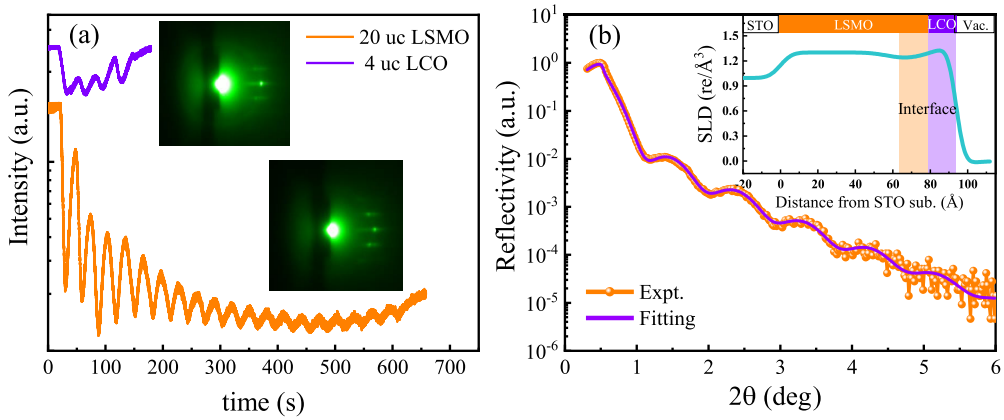

FIG. 1. (a) *In situ* RHEED patterns during growth of the 4LCO/20LSMO heterostructure. (b) X-ray reflectivity data and the fit of the 4LCO/20LSMO heterostructure. Insets: x-ray SLD depth profile.

superexchange interaction (e_g^0-O-e_g^2 type) triggered by the interfacial electron transfer process.

II. MATERIALS AND METHODS

Single TiO_2-terminated $SrTiO_3$ (STO) substrates were obtained by etching with a standard buffered oxide etch solution and subsequent annealing at 950 °C for 1 h [18]. The single layer of LCO, LSMO, and LCO/LSMO heterostructures was grown on (001) STO substrates by a homemade laser molecular beam epitaxy using a KrF excimer laser operating at 248 nm. The laser fluence and repetition rate were 1.5 J/cm^2 and 4 Hz, respectively. The typical substrate temperature was 600 °C, and the oxygen partial pressure was 0.15 mbar. The thickness of each sublayer is precisely controlled by *in situ* reflection high-energy electron diffraction (RHEED). Both the good oscillation and sharp RHEED diffraction patterns ensure the layer-by-layer growth of the films with precise control at the single unit cell (u.c.) level [in Fig. 1(a)].

The sample's layered structure and thickness were characterized by x-ray reflectometry (XRR) using a high-resolution Malvern Panalytical diffractometer ($\lambda = 1.5406$ Å). Further XRR fitting was conducted by GENX software to decipher the individual thickness of LCO and LSMO. The magnetic property measurements were carried out by a superconducting quantum interference device (SQUID; Quantum Design, MPMS 3) magnetometer. The magnetization (M-H) loops for the heterostructure were measured at $T = 10$ K. The sample magnetization was acquired by subtracting the diamagnetic contribution from the STO substrate. After 5000 Oe field cooling to 2 K, the temperature-dependent magnetization (M-T) of the sample was measured during warm-up upon processing with applied magnetic field 500 Oe along [001] orientation. To shed light on the interfacial magnetic contributions to the ferromagnetic state observed in heterojunctions, we performed XAS as well as XMCD measurements at the 3d transition metal (Co, Mn) $L_{2,3}$ edges as a function of temperature. Using the horizontal linear polarized x ray, the XAS was measured in total electron yield mode to determine the valence states of Co and Mn ions. The dichroic XMCD signal was recorded as the difference in the x-ray absorption spectra measured under a magnetic field of $\mu_0 H = \pm 7$ T applied perpendicular to the sample surface, with a parallel (σ^+)/antiparallel (σ^-) circular helicity beam. The XAS and XMCD measurements were conducted at the beamlines MCD-A and MCD-B (Soochow Beamline for Energy Materials) at National Synchrotron Radiation Laboratory (NSRL) and the VEKMAG end station at the PM-2 beamline of the Bessy II electron storage ring operated by the Helmholtz-Zentrum Berlin [19], respectively.

III. RESULTS AND DISCUSSION

For the 4-u.c. LCO/20-u.c. LSMO (4LCO/20LSMO) heterostructure, the thicknesses of the LSMO and LCO layers are extracted from the XRR characterization in Fig. 1(b) and are 79 ± 1 and 15 ± 1 Å, respectively. These results are consistent with the c-axis lattice constant of 3.94 and 3.75 Å for LCO and LSMO, respectively. The x-ray scattering length density (SLD) depth profile in Fig. 1(b) reveals a slight decrease in the density of LSMO within a thickness range of $64-79 \pm 1$ Å, indicating a lattice distortion of LSMO within a range of approximately four u.c. at the interface. The RHEED and XRR results demonstrate that the LCO/LSMO heterostructure interface exhibits atomic-level flatness, which forms the basis for strong interfacial effects.

The M-T curve of the 4LCO/20LSMO heterostructure is shown in Fig. 2(a). Two ferromagnetic transition points are extracted at approximately 320 and 190 K, according to the quantitative fitting based on the expression $M \propto (1-T/T_C)^\beta$ [20]. As depicted in Fig. 2(b), the T_C of single LSMO and LCO films are observed to be approximately 320 and 76 K, respectively, aligning with the reported work [15,21]. Consequently, the ferromagnetic transition at approximately 320 K can be attributed to the thicker LSMO film layer, and the slight decrease from 370 K for bulk LSMO [22] is due to the reduced thickness [23–25]. In addition, the T_C of 190 K significantly exceeds that of 76 K for the single LCO film, suggesting that the interfacial ferromagnetic state contributes to this ferromagnetic transition. At the interface of transition metal oxide heterostructures, significant charge-transfer effects often occur with distortion of the lattice structure [23,26]. Therefore, a plausible mechanism for the interfacial ferromagnetic state is interfacial charge transfer and exchange coupling at the

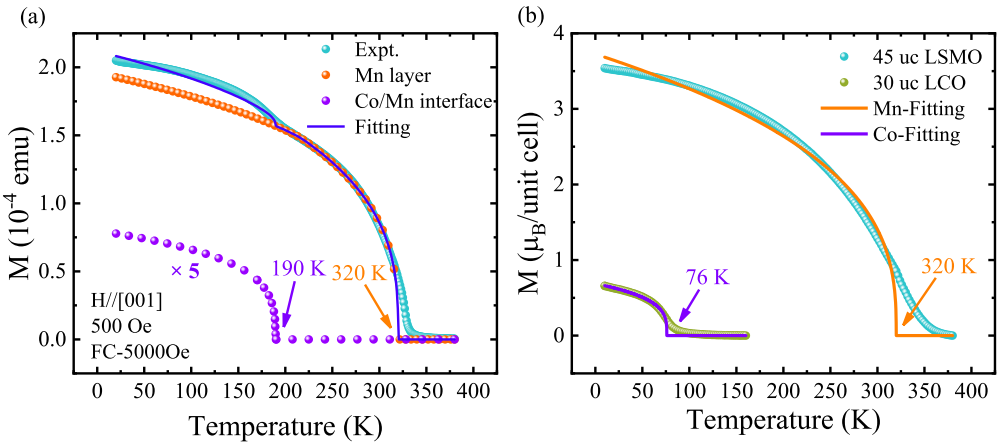

FIG. 2. Temperature-dependent magnetization. (a) *M-T* curve and the fit of the 4LCO/20LSMO heterostructure, which is contributed by both the LSMO single layer with a transition temperature of 320 K (orange balls) and the LCO/LSMO interface with a transition temperature of 190 K (purple balls). (b) *M-T* curves and the fit of the single LCO and LSMO films.

LCO/LSMO interface. Based on the band structure of LSMO and LCO [26,27], electrons are expected to transfer from Mn ions to Co ions due to the significant mismatch of Fermi levels at the heterointerface, resulting in the reduction of Co ions from +3 to +2 valence.

Further XAS analysis of Co *L* edges in Fig. 3 confirms the expected interfacial charge transfer from LSMO to LCO, as evidenced by the appearance of Co^{2+}. As marked by the black dashed line, a distinct "shoulder" is observed on the left of the L_3 absorption edge (near 777 eV), contrasting with the LCO/STO heterojunction, which indicates the presence of Co^{2+} ions [28,29]. Moreover, a clear "shoulder" observed on the right side of the L_3 absorption edge (near 781 eV)

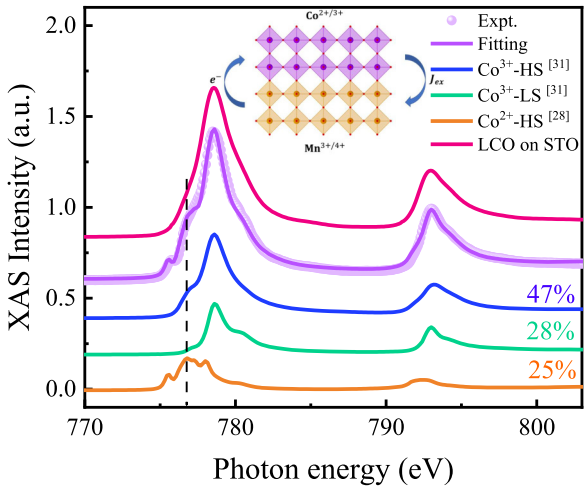

FIG. 3. Normalized isotropic XAS spectra at the Co $L_{2,3}$ edges of the 4LCO/20LSMO heterostructure together with reference spectra for various valent Co ions, indicating that approximately 25% of Co^{3+} is converted into Co^{2+} at the interface. The 40-u.c. LCO film grown on the STO substrate was used as a comparison. Here, the profile of reference Co^{2+} is obtained by measuring CoO, and those of Co^{3+} HS and Co^{3+} LS correspond to the experimental spectroscopy of two different cobaltates, $Sr_2Co_{0.5}Ir_{0.5}O_4$ and $NdCaCoO_4$, respectively. Insets: schematic charge transfer at the LCO/LSMO interface.

suggests the presence of a certain amount of Co^{3+} − LS ions [15,23,30]. Given multiple states for the Co element in LCO, their concentrations were obtained by linearly combining different reference components, including Co^{3+} HS, Co^{3+} LS, and Co^{2+} HS. Here, the profile of reference Co^{2+} is obtained by measuring CoO [28], and those of Co^{3+} HS and Co^{3+} LS correspond to the experimental spectroscopy of two different cobaltates, $Sr_2Co_{0.5}Ir_{0.5}O_4$ and $NdCaCoO_4$, respectively [31]. The fit shows the presence of approximately 47% Co^{3+} − HS ions, and 25% Co^{2+}-HS ions, leaving only 28% of nonmagnetic Co^{3+}-LS ions. It should be emphasized that the Co^{3+}-HS state and the Co^{2+}-HS ions favor magnetic ordering and should therefore enhance the exchange interaction between Mn and Co at the interface [17]. Analogous charge-transfer behavior was also observed at the interface of the LCO/STO heterostructures [23], where the charge-transfer phenomenon is confined to appear in only a few cell layers around the interface. Thus, we can conclude that the Mn-Co ferromagnetic exchange interactions based on charge transfer occur only at the LCO/LSMO interface, as illustrated schematically in the inset of Fig. 3.

The Co *L*-edge and Mn *L*-edge XMCD spectra are further separately characterized to verify the magnetic nature at the LCO/LSMO interface. The total electron yield signal of XMCD mainly originates from the sample surface with a depth of 3–5 nm, corresponding to the total thickness of the LCO/LSMO interfacial layer. Therefore, the magnetic response measured by XMCD primarily originates from the Co and Mn ions near the interface. Figure 4(a) illustrates the XMCD signals measured at different temperatures for Co ions (top) and Mn ions (bottom). Compared to bulk LCO [29], a highly enhanced XMCD signal at the Co *L* edge can be observed for the LCO/LSMO sample. This is consistent with that in the $LaTiO_3/LaCoO_3/LaTiO_3$ heterostructure [30], where charge transfer at the interface enhanced the LCO magnetism by a factor of 4–6. The XMCD sum rule was used to quantitatively estimate the magnetization intensity [32,33], and the calculated values were corrected according to the beamline polarization of 77% (PM-2 VEKMAG). In our analysis of the Co moments, we utilized a hole count $n_h = 3.5$, which

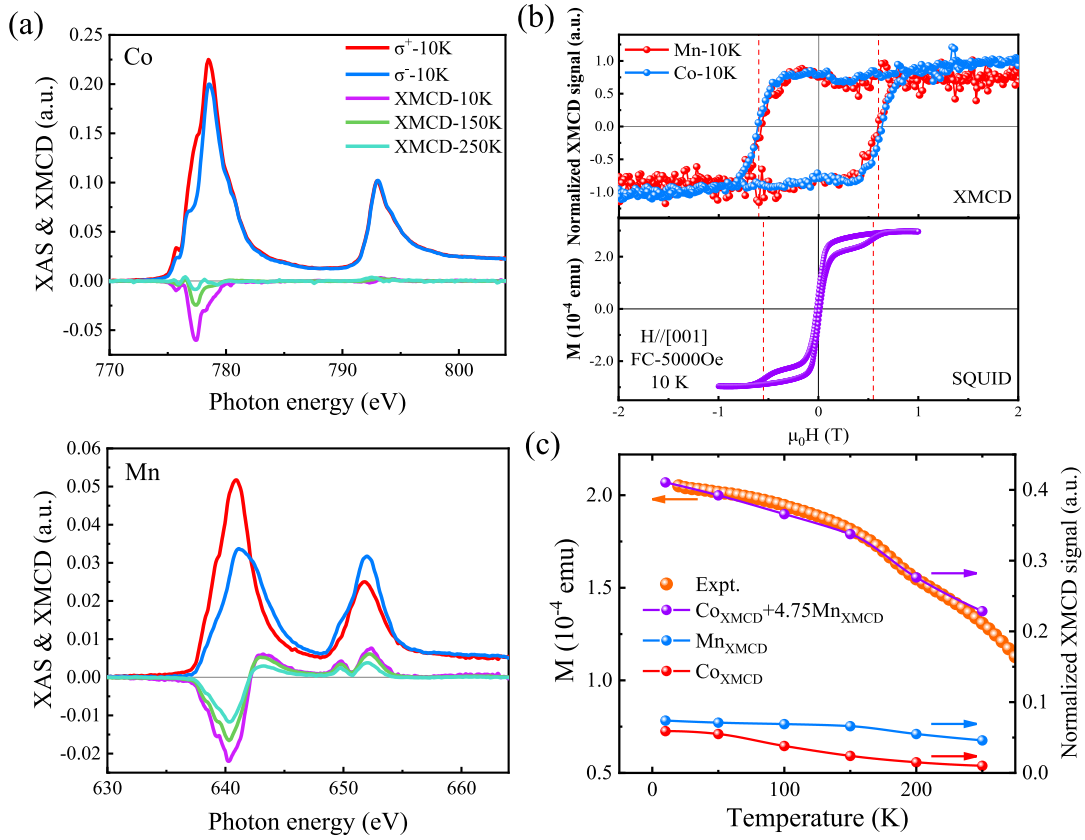

FIG. 4. (a) Co (Mn) edge XMCD spectra obtained at 10, 150, and 250 K with the external field of ±7 T. Remarkable XMCD signals indicate magnetic coupling at the LCO/LSMO interface. (b) Comparison between the elemental-specific hysteresis of the LCO/LSMO interface extracted from XMCD and the overall hysteresis of the 4LCO/20LSMO heterostructure extracted from a SQUID. (c) Temperature-dependent magnetism extracted from XMCD and a SQUID indicates that the ferromagnetic transition occurring at approximately 190 K can be attributed to Mn-Co coupling at the interface.

is considered that the XAS fitting showed a mixture of +2 and +3 valence Co ions in the LCO films. The total magnetic moment of Co is determined to be 0.67 μ_B/Co at 10 K and $\mu_0 H = 7$ T, which is comparable to the magnetic moment of 0.79 μ_B/Co observed in LCO single films obtained from the above SQUID magnetometry results [in Fig. 2(b)]. For Mn, we employed $n_h = 6.0$, which is intermediate between the values of 5.5 for Mn^{3+} and 6.4 for Mn^{4+} [34]. The moment of Mn is determined to be 4.33 μ_B/Mn, which is notably larger than the saturation magnetic moment of 3.67 μ_B/Mn for single LSMO films [in Fig. 2(b)]. It should be noted that a correction factor of 1.7 was applied to account for the mixing of the L_3 and L_2 edges of Mn [35]. This implies a remarkable alteration in the magnetic properties of interfacial Mn and Co ions due to the interplay of charge transfer and orbital hybridization. The XMCD of Co ions gradually decreases with increasing temperature, retaining a larger signal at 150 K and approaching zero at 250 K. Furthermore, the XMCD signals of Co and Mn ions at the L_3 absorption edge are both negative, implying that the coupling directions between Co and Mn ions across the interface are parallel; that is, they belong to ferromagnetic coupling. XMCD characteristics indicate that a high-temperature ferromagnetic LCO was induced in the LCO/LSMO interface.

By sweeping the applied magnetic field, we can measure the hysteresis loops of Co and Mn ions using the XMCD signal, as shown in Fig. 4(b). Co and Mn ions exhibit the same hysteresis characteristics with coercivity fields of the same magnitude corresponding to the *M-H* curve measured by the SQUID. The synchronous magnetic response of Co and Mn ions to the external magnetic field again strongly corroborates the emergence of an unusual ferromagnetic state within the LCO/LSMO interface, which exhibits distinct coercivity and magnetic anisotropy from the deeper LSMO layer. Figure 4(c) shows the variation characteristics of the XMCD signal at more temperatures and investigates the *M-T* characteristics of Co and Mn ions. By combining the XMCD signals of Co and Mn ions in a proper ratio, the resulting ferromagnetic signal characteristics with temperature match well with the *M-T* transition characteristics measured by a SQUID. The mutual consistency of the XMCD and SQUID signals in terms of both microscopic magnetic moments and macroscopic magnetism demonstrates the emergence of an unusual ferromagnetic state within the LCO/LSMO interface, which is mediated by charge transfer and orbital hybridization across the interface, inducing a high-temperature ferromagnetic LCO layer with a T_C up to 190 K.

We conducted a comprehensive analysis of the potential ferromagnetic exchange coupling between Mn and Co ions in the LCO/LSMO interface. Although the actual magnetic interactions could be complex due to the different spin and charge states of Co ions formed at the interface, as shown

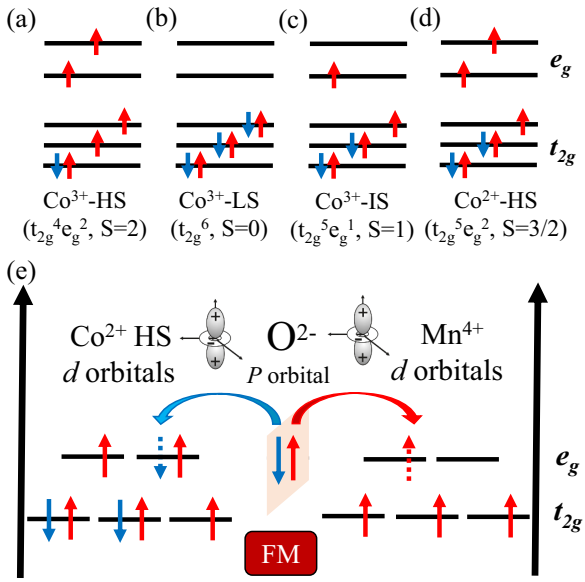

FIG. 5. Different spin states of Co^{3+} ions (a)–(c) and Co^{2+}-HS states (d). (e) Ferromagnetic coupling from Mn^{4+}-O-Co^{2+} superexchange interaction (e_g^0-O-e_g^2 type) at the LCO/LSMO interface.

in Figs. 5(a)–5(d), the dominant components were extracted based on previous XAS and XMCD analyses. For instance, by examining the valence state of Co ions in Fig. 3, it is discovered that approximately 25% of Co^{2+} HS exists in the LCO film. This electronic state is a result of the charge transfer from Mn to Co at the interface and plays a crucial role in the resulting ferromagnetic coupling. It is generally accepted that the FM insulating ground state of the LCO film is established via the superexchange interaction within the HS-LS-HS Co^{3+} configuration. However, this weak interaction easily vanishes when the Co^{2+} HS reaches a threshold ratio of ∼12.5% [15], since the exchange coupling between two Co^{2+}'s with a half-filled e_g orbital turns out to be strong and antiferromagnetic (AFM). This explains the disappearance of the transition temperature around 85 K and implies that the ferromagnetic (FM) transition around 190 K of the LCO/LSMO interface was dominated by the interfacial Mn^{4+}-O-Co^{2+} superexchange, as shown in Fig. 5(e). The superexchange interaction mediated by oxygen anions between Mn^{4+} ions with empty e_g orbitals and Co^{2+}-HS ions with half-filled e_g orbitals will induce an e_g^0-O-e_g^2 type ferromagnetic order [36–39], according to the Goodenough-Kanamori-Anderson rules. As a result, a high-temperature ferromagnetic state with $T_C \approx 190$ K was induced in the LCO film.

To address the Mn^{4+}-O-Co^{2+} superexchange within the current literature concerning theoretical calculations pertaining to the LCO/LSMO interface layer, we performed a density functional theory (DFT) simulation within the generalized gradient approximation Perdew-Burke-Ernzerhof (PBE) functional and the projector augmented wave method as implemented in the Vienna *ab initio* simulation package (VASP) [40,41]. These calculations enabled us to theoretically elucidate the magnetic ground state of the interface layer. For simplicity, we constructed an LCO (two u.c.)/LSMO (two u.c.) interface structure; the lattice constants are $a = b = 3.89$ Å and $c = 3.94/3.75$ Å (LCO/LSMO) during calculation. To consider the 33% Sr dopants and several magnetic configurations, we built a $2 \times 3 \times 1$ supercell. The electronic correlations on Co/Mn-3*d* are included by the DFT+*U* method with $U = 3.0$ eV. The kinetic energy cutoff is set to 500 eV, and the Brillouin zone is sampled with $4 \times 3 \times 2$ Monkhorst-Pack k grids for PBE calculations. The partial density of states (PDOS) result is shown in Fig. 6, the orange dashed line of Mn-t_{2g} orbitals reveals the fully occupied up channel and unoccupied down channel, and the green dashed line of Co-t_{2g} orbitals reveals the fully occupied up channel and the partially occupied down channel. The solid line, representing the e_g orbitals of Mn and Co, exhibits an apparent ferromagnetic interaction between Mn-e_g and Co-e_g. The results of the PDOS hint at an electronic configuration with Co^{2+}-HS state and Mn^{4+}-HS state as shown in Fig. 5(e). Due to the hybridization between Mn/Co-3*d* and O-2*p*, which further induces the interlayer superexchange interaction, the calculated magnetic moment of the ferromagnet is about 3.3 μ_B for Mn and 2.0 μ_B for Co. To validate the magnetic ground state, we also explored the relative formation energy of the G-AFM, C-AFM, and A-AFM configurations related to the FM configuration, which are 0.421, 0.284, and 0.198 eV, respectively. The energy gap between the ferromagnet and the antiferromagnet is about 420 meV/Co, indicating the dominant interaction between the transition metal atoms in the LCO/LSMO interface is FM in nature. Combined with the results of the magnetic moment, total energy, and PDOS of LSMO/LCO, we suggest that the ferromagnetic mechanism summarized in Fig. 5(e) is reasonable.

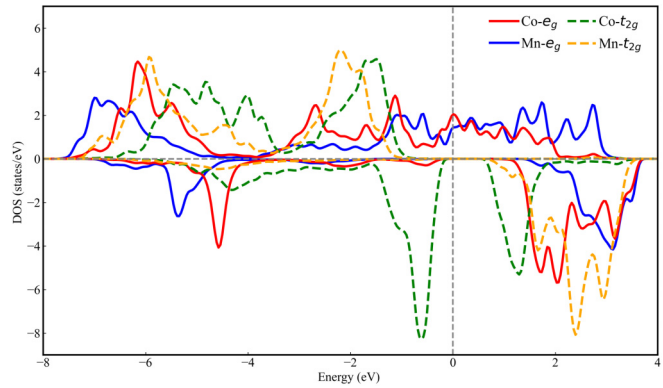

FIG. 6. Atom projected density of states of 2LCO/2LSMO interface for FM spin configuration in GGA+*U* formalism. The positive (negative) values of DOS indicate spin-up (spin-down) channels, and the dashed vertical line at 0 eV indicates the Fermi energy level.

IV. CONCLUSION

In summary, our research concentrated on the magnetic properties of the 4LCO/20LSMO heterostructure grown on the STO substrates. The heterojunction is made up of two distinct magnetic components: the complex LCO/LSMO interface layer and the thicker LSMO film layer. A high-temperature ferromagnetic state with a T_C of approximately 190 K is produced at the LCO/LSMO interface, which is much higher than the T_C of a single LCO film. This phenomenon is primarily attributed to significant charge transfer and orbital

hybridization across the interface, which resulted in a ferromagnetic superexchange interaction between Mn^{4+} and Co^{2+} ions that is mediated by oxygen anions. Finally, we further examined the magnetic moments and PDOS of Mn and Co using DFT calculations to provide theoretical support for our mechanism. Our findings offer valuable insights and design concepts for enhancing the T_C of LCO films and highlight the intriguing physics and potential applications of transition metal oxide heterostructures influenced by interfacial effects.

The data that support the plots within this paper as well as other findings of this study are available from the corresponding author upon reasonable request.

ACKNOWLEDGMENTS

This work was supported by National Natural Science Foundation of China (Grants No. 11974325, No. 52272095, and No. 12275272), Fundamental Research Funds for the Central Universities (Grants No. WK2030000035, No. WK2310000104, and No. WK2310000106), and Collaborative Innovation Program of Hefei Science Center, CAS (Grant No. CX2310000177). The authors would like to thank beamlines MCD-A and MCD-B (Soochow Beamline for Energy Materials) at NSRL and VEKMAG end station at the Bessy II electron storage ring operated by the Helmholtz-Zentrum Berlin für Materialia for the synchrotron beamtime.

The authors declare no conflict of interest.

[1] Y. Z. Chen, N. Bovet, F. Trier, D. V. Christensen, F. M. Qu, N. H. Andersen, T. Kasama, W. Zhang, R. Giraud, J. Dufouleur *et al.*, A high-mobility two-dimensional electron gas at the spinel/perovskite interface of γ-Al_2O_3/$SrTiO_3$, Nat. Commun. **4**, 1371 (2013).

[2] Z. Q. Liu, C. J. Li, W. M. Lü, X. H. Huang, Z. Huang, S. W. Zeng, X. P. Qiu, L. S. Huang, A. Annadi, J. S. Chen *et al.*, Origin of the two-dimensional electron gas at $LaAlO_3$/$SrTiO_3$ interfaces: The role of oxygen vacancies and electronic reconstruction, Phys. Rev. X **3**, 021010 (2013).

[3] M. L. Liu, X. S. Li, L. Li, L. X. Li, S. G. Zhao, K. G. Lu, K. Chen, J. L. Zhu, T. Zhou, C. L. Hu *et al.*, Continuous photothermal and radiative cooling energy harvesting by VO_2 smart coatings with switchable broadband infrared emission, ACS Nano **17**, 9501 (2023).

[4] J. Matsuno, N. Ogawa, K. Yasuda, F. Kagawa, W. Koshibae, N. Nagaosa, Y. Tokura, and M. Kawasaki, Interface-driven topological Hall effect in $SrRuO_3$-$SrIrO_3$ bilayer, Sci. Adv. **2**, e1600304 (2016).

[5] X. Hua, F. Meng, Z. Huang, Z. Li, S. Wang, B. Ge, Z. Xiang, and X. Chen, Tunable two-dimensional superconductivity and spin-orbit coupling at the EuO/$KTaO_3$(110) interface, npj Quantum Mater. **7**, 97 (2022).

[6] M. Gibert, P. Zubko, R. Scherwitzl, J. Iñiguez, and J. M. Triscone, Exchange bias in $LaNiO_3$-$LaMnO_3$ superlattices, Nat. Mater. **11**, 195 (2012).

[7] C. He, A. J. Grutter, M. Gu, N. D. Browning, Y. Takamura, B. J. Kirby, J. A. Borchers, J. W. Kim, M. R. Fitzsimmons, X. Zhai *et al.*, Interfacial ferromagnetism and exchange bias in $CaRuO_3$/$CaMnO_3$ superlattices, Phys. Rev. Lett. **109**, 197202 (2012).

[8] S. Bhowal and S. Satpathy, Electronic structure and anomalous Hall effect in the ferromagnetic 3*d*/5*d* superlattice $SrMnO_3$/$SrIrO_3$, Phys. Rev. B **99**, 245145 (2019).

[9] D. Lan, B. Chen, L. Qu, F. Jin, Z. Guo, L. Xu, K. Zhang, G. Gao, F. Chen, S. Jin *et al.*, Interfacial engineering of ferromagnetism in epitaxial manganite/ruthenate superlattices via interlayer chemical doping, ACS Appl. Mater. Interfaces **11**, 10399 (2019).

[10] Y. Naito and K. Suetake, Application of ferrite to electromagnetic wave absorber and its characteristics, IEEE Trans. Microwave Theory Tech. **19**, 65 (1971).

[11] P. Tenaud, A. Morel, F. Kools, J. M. Le Breton, and L. Lechevallier, Recent improvement of hard ferrite permanent magnets based on La-Co substitution, J. Alloy. Compd. **370**, 331 (2004).

[12] R. F. Ziolo, E. P. Giannelis, B. A. Weinstein, M. P. Ohoro, B. N. Ganguly, V. Mehrotra, M. W. Russell, and D. R. Huffman, Matrix-mediated synthesis of nanocrystalline gamma-Fe_2O_3: A new optically transparent magnetic material, Science **257**, 219 (1992).

[13] J. S. Moodera, X. Hao, G. A. Gibson, and R. Meservey, Electron-spin polarization in tunnel-junctions in zero applied field with ferromagnetic EuS barriers, Phys. Rev. Lett. **61**, 637 (1988).

[14] S. Li, J. Wang, Q. Zhang, M. A. Roldan, S. Lin, Q. Jin, S. Chen, Z. Wu, C. Wang, C. Ge *et al.*, Maximization of ferromagnetism in $LaCoO_3$ films by competing symmetry, Phys. Rev. Mater. **3**, 114409 (2019).

[15] D. C. Meng, H. L. Guo, Z. Z. Cui, C. Ma, J. Zhao, J. B. Lu, H. Xu, Z. C. Wang, X. Hu, Z. P. Fu *et al.*, Strain-induced high-temperature perovskite ferromagnetic insulator, Proc. Natl. Acad. Sci. USA **115**, 2873 (2018).

[16] S. Q. Chen, J. Y. Chang, Q. H. Zhang, Q. Y. Li, T. Lin, F. Q. Meng, H. L. Huang, Y. Y. Si, S. W. Zeng, X. M. Yin *et al.*, Spin state disproportionation in insulating ferromagnetic $LaCoO_3$ epitaxial thin films, Adv. Sci. **10**, 2303630 (2023).

[17] M. Merz, P. Nagel, C. Pinta, A. Samartsev, H. von Lohneysen, M. Wissinger, S. Uebe, A. Assmann, D. Fuchs, and S. Schuppler, X-ray absorption and magnetic circular dichroism of $LaCoO_3$, $La_{0.7}Ce_{0.3}CoO_3$, and $La_{0.7}Sr_{0.3}CoO_3$ films: Evidence for cobalt-valence-dependent magnetism, Phys. Rev. B **82**, 174416 (2010).

[18] A. Biswas, C. H. Yang, R. Ramesh, and M. H. Jeong, Atomically flat single terminated oxide substrate surfaces, Prog. Surf. Sci. **92**, 117 (2017).

[19] T. Noll and F. Radu, in *Proceedings of Mechanical Engineering Design of Synchrotron Radiation Equipment and Instrumentation Conference (MEDSI '16)* (JACoW, Geneva, Switzerland, 2017), pp. 370–373.

[20] C. Kittel, *Introduction to Solid State Physics (8th ed.)* (John Wiley & Sons, New York, 2004), pp. 321–357.

[21] F. Tsui, M. C. Smoak, T. K. Nath, and C. B. Eom, Strain-dependent magnetic phase diagram of epitaxial $La_{0.67}Sr_{0.33}MnO_3$ thin films, Appl. Phys. Lett. **76**, 2421 (2000).

[22] R. Peng, H. C. Xu, M. Xia, M. Xia, J. F. Zhao, X. Xie, D. F. Xu, B. P. Xie, and D. L. Feng, Tuning the dead-layer behavior of $La_{0.67}Sr_{0.33}MnO_3/SrTiO_3$ via interfacial engineering, Appl. Phys. Lett. **104**, 081606 (2014).

[23] W. Niu, Y. W. Fang, X. Q. Zhang, Y. K. Weng, Y. D. Chen, H. Zhang, Y. L. Gan, X. Yuan, S. J. Zhang, J. B. Sun *et al.*, Charge-transfer-induced multivalent states with resultant emergent magnetism in transition-metal oxide heterostructures, Adv. Electron. Mater. **7**, 2000803 (2021).

[24] F. Sandiumenge, J. Santiso, L. Balcells, Z. Konstantinovic, J. Roqueta, A. Pomar, J. P. Espinos, and B. Martinez, Competing misfit relaxation mechanisms in epitaxial correlated oxides, Phys. Rev. Lett. **110**, 107206 (2013).

[25] L. Li, Y. Y. Ji, Z. Y. Diao, J. D. Zhang, and Z. L. Liao, Toward ultrathin ferromagnetic metal of (110) $La_{2/3}Sr_{1/3}MnO_3$ thin films, Appl. Phys. Lett. **117**, 122404 (2020).

[26] M. Meng, Y. Sun, Y. Li, Q. An, Z. Wang, Z. Lin, F. Yang, X. Zhu, P. Gao, and J. Guo, Three dimensional band-filling control of complex oxides triggered by interfacial electron transfer, Nat. Commun. **12**, 2447 (2021).

[27] F. R. Han, X. B. Chen, J. N. Zhang, J. Zhang, J. H. Song, H. Zhang, H. R. Zhang, X. Yan, Q. H. Zhang, L. Gu *et al.*, Spin reorientation at (110)-$La_{2/3}Sr_{1/3}MnO_3/LaCoO_3$ interfaces by orbital/charge reconstruction, APL Mater. **8**, 021113 (2020).

[28] S. I. Csiszar, M. W. Haverkort, Z. Hu, A. Tanaka, H. H. Hsieh, H. J. Lin, C. T. Chen, T. Hibma, and L. H. Tjeng, Controlling orbital moment and spin orientation in CoO layers by strain, Phys. Rev. Lett. **95**, 187205 (2005).

[29] M. W. Haverkort, Z. Hu, J. C. Cezar, T. Burnus, H. Hartmann, M. Reuther, C. Zobel, T. Lorenz, A. Tanaka, N. B. Brookes *et al.*, Spin state transition in LaCoO3 studied using soft x-ray absorption spectroscopy and magnetic circular dichroism, Phys. Rev. Lett. **97**, 176405 (2006).

[30] G. Araizi-Kanoutas, J. Geessinck, N. Gauquelin, S. Smit, X. H. Verbeek, S. K. Mishra, P. Bencok, C. Schlueter, T. L. Lee, D. Krishnan *et al.*, Co valence transformation in isopolar $LaCoO_3/LaTiO_3$ perovskite heterostructures via interfacial engineering, Phys. Rev. Mater. **4**, 026001 (2020).

[31] S. C. Haw, Z. W. Hu, H. J. Lin, J. M. Lee, H. Ishii, N. Hiraoka, A. Meléndez-Sans, A. C. Komarek, L. H. Tjeng, K. Chen *et al.*, Unusual mixed spin-state of Co^{3+} in the ground state of $LaSrCoO_4$: Combined high-pressure and high-temperature study, J. Alloy. Compd. **862**, 158050 (2021).

[32] B. T. Thole, P. Carra, F. Sette, and G. van der Laan, X-ray circular dichroism as a probe of orbital magnetization, Phys. Rev. Lett. **68**, 1943 (1992).

[33] C. T. Chen, Y. U. Idzerda, H. J. Lin, N. V. Smith, G. Meigs, E. Chaban, G. H. Ho, E. Pellegrin, and F. Sette, Experimental confirmation of the x-ray magnetic circular-dichroism sum-rules for iron and cobalt, Phys. Rev. Lett. **75**, 152 (1995).

[34] T. Saitoh, A. E. Bocquet, T. Mizokawa, and A. Fujimori, Systematic variation of the electronic-structure of 3D transition-metal compounds, Phys. Rev. B **52**, 7934 (1995).

[35] C. Piamonteze, M. Gibert, J. Heidler, J. Dreiser, S. Rusponi, H. Brune, J. M. Triscone, F. Nolting, and U. Staub, Interfacial properties of $LaMnO_3/LaNiO_3$ superlattices grown along (001) and (111) orientations, Phys. Rev. B **92**, 014426 (2015).

[36] A. Banerjee, J. Sannigrahi, S. Giri, and S. Majumdar, Magnetization reversal and inverse exchange bias phenomenon in the ferrimagnetic polycrystalline compound Er_2CoMnO_6, Phys. Rev. B **98**, 104414 (2018).

[37] P. A. Joy, Y. B. Khollam, and S. K. Date, Spin states of Mn and Co in $LaMn_{0.5}Co_{0.5}O_3$, Phys. Rev. B **62**, 8608 (2000).

[38] H. L. Wang, J. Gazquez, C. Frontera, M. F. Chisholm, A. Pomar, B. Martinez, and N. Mestres, Spontaneous cationic ordering in chemical-solution-grown La_2CoMnO_6 double perovskite thin films, NPG Asia Mater. **11**, 44 (2019).

[39] J. T. Zhang, X. M. Lu, X. Q. Yang, J. L. Wang, and J. S. Zhu, Origins of $\uparrow\uparrow\downarrow\downarrow$ magnetic structure and ferroelectricity in multiferroic Lu_2CoMnO_6, Phys. Rev. B **93**, 075140 (2016).

[40] J. P. Perdew, K. Burke, and M. Ernzerhof, Generalized gradient approximation made simple, Phys. Rev. Lett. **77**, 3865 (1996).

[41] G. Kresse and J. Furthmüller, Efficient iterative schemes for *ab initio* total-energy calculations using a plane-wave basis set, Phys. Rev. B **54**, 11169 (1996).